

Additional studies of the anomalous $l + \cancel{E}_T + 2, 3$ jet events observed by CDF

G. Apollinari,² M. Barone,³ W. Carithers,⁴ T. Dorigo,⁶ I. Fiori,⁶ P. Giromini,³ F. Happacher,³
M. Kruse,¹ S. Miscetti,³ A. Parri,³ F. Ptohos,³ and Y. Srivastava⁵

¹ *Duke University, Durham, North Carolina 27708*

² *Fermi National Accelerator Laboratory, Batavia, Illinois 60510*

³ *Laboratori Nazionali di Frascati, Istituto Nazionale di Fisica Nucleare, I-00044 Frascati, Italy*

⁴ *Ernest Orlando Lawrence Berkeley National Laboratory, Berkeley, California 94720*

⁵ *Northeastern University, Boston, Massachusetts 02115*

⁶ *Universita di Padova, Istituto Nazionale di Fisica Nucleare, Sezione di Padova, I-35131 Padova, Italy*

We present additional studies of the kinematics of the anomalous events observed by the CDF experiment. These events contain a high- p_T lepton, large transverse missing energy (\cancel{E}_T), and 2 or 3 high- E_T jets, one of which contains both a displaced secondary vertex and a soft lepton. Previous articles detailed the selection and the kinematic properties of these events. In the present paper, we use several phenomenological approaches to model these data and to estimate their production cross section.

PACS number(s): 13.85.Qk, 13.20.He, 14.80.Ly

I. INTRODUCTION

The CDF experiment has observed [1] an excess of events in the $W + 2$ and $W + 3$ jet topologies in which the presumed heavy-flavor jet contains a lepton in addition to a secondary vertex. The rate of these events (13 observed) is larger than what is predicted by the simulation of known standard model (SM) processes (4.4 ± 0.6 events expected, including single and pair production of top quarks). The kinematical properties of these events are not

consistent with what is expected if the excess were due to a statistical fluctuation of the SM contributions [1,2]. This small sample of events has been isolated in a detailed examination of the heavy-flavor content of the $W + \text{jet}$ data sample collected by the CDF experiment during the 1992-1995 collider run at the Fermilab Tevatron. Jets with heavy-flavor hadrons are identified using the SECVTX algorithm that reconstructs secondary vertices (SECVTX tags), the jet-probability (JPB) algorithm [3], and the SLT algorithm that identifies leptons produced in the decay of b and c -hadrons (SLT tags). Jets containing both a SECVTX and SLT tag (supertag) are referred to as superjets. The data set, the analysis tools and the Monte Carlo simulations used in this study are the same as those described in Sec. IV of Ref. [1]. The characteristics of the 13 events with a superjet are listed in Tables XVI and XVII of Ref. [1].

We are not aware of any model for new physics which incorporates the production and decay properties necessary to explain all features of the 13 events with a superjet. In the absence of a suitable theoretical model, in this paper we investigate several hypotheses with the purpose of evaluating the production cross section of these anomalous events. For this purpose, we use tools, names and ideas developed for specific models, none of which can be supported or excluded at the current time because of the limited statistics of the data. In Sec. II we investigate the hypothesis that superjets are due to the production and weak decay of a light spin-0 quark (scalar quark, \tilde{q}). In order to estimate the size of the anomalous contribution we fit the yields of $W + \text{jet}$ events with different types of tags with a SM simulation implemented with the pair production of a scalar quark and a b quark with large invariant mass ($\simeq 220 \text{ GeV}/c^2$). The fit result shows that the observed tagging rates can be reasonably described with this simple addition, and provides a first indication of how much the CDF measurement [4] of the $t\bar{t}$ production cross section is impacted by the presence of events with a superjet. In Sec. III we use several simulations based upon the salient features of the data in order to evaluate the detector acceptance for events with a superjet and estimate their production cross section. Section IV summarizes our conclusions.

II. ESTIMATE OF THE SIZE OF THE ANOMALOUS PRODUCTION

An interpretation in terms of new physics of the superjet properties, which are described in Sec. IX of Ref. [1], would require the production of a low-mass, strongly interacting object, decaying semileptonically with a branching ratio close to 1 and with a lifetime of the order of a picosecond. The low mass is required by the fact that the SECVTX and SLT tags are contained in a cone of radius 0.4 in the $\eta - \phi$ space around the jet axis. The request that the object is strongly interacting is motivated by the fact that several tracks in the superjet point directly to the primary vertex, suggesting an emission of gluons during the evolution prior to the decay. The large semileptonic branching ratio, finally, is required to explain the large fraction of soft lepton tags in jets tagged by SECVTX.

Since there are no experimental limits on the existence of a charge-1/3 scalar quark with mass smaller than 7.4 GeV/c² [5–7], the supersymmetric partner of the bottom quark is a potential candidate. In order to explain the observed rate of supertags, one possible assumption is that this scalar quark has three-body decay modes to quarks mediated by heavy gauge fermions χ ($m_\chi \geq m_{\tilde{b}}$) and that $\chi \rightarrow l\tilde{\nu}$ is the only allowed decay. As an example, in this study we use the ansatz that superjets are due to the production and decay into $lc\tilde{\nu}$ of a scalar quark \tilde{b} with a mass of 3.6 GeV/c² and a lifetime of 1.0 ps; the scalar neutrino is assumed to be massless. Such a scalar quark is not ruled out by the CLEO collaboration [8] if its decay matrix element results in a lepton spectrum softer than three-body phase space, as is the case for the matrix element used by us (see Appendix A). Even if such a \tilde{b} quark were ruled out, we would retain this simple model, which fits the data reasonably well, as a working hypothesis to estimate the production cross section of the anomalous events. In fact, many slightly different conjectures ($m_{\tilde{\nu}}$ in the range of a few GeV/c² and $2 \leq m_{\tilde{b}} - m_c - m_{\tilde{\nu}} \leq 5$ GeV/c²) are still not excluded by any data analysis and, because of the limited statistics of the CDF data and the large transverse energy of the superjets ($\simeq 60$ GeV), they also provide a reasonable modeling of the superjet properties [9]. We also note that we assume the presence of a c quark in the \tilde{b} decay but this assumption

is not required to fit any of the superjet properties.

The estimate of the production cross section of the events with a superjet requires the knowledge of the tagging efficiencies and the detector acceptance, which in turn depend on the kinematics of the data. For example, the acceptance is sensitive to the pseudo-rapidity and transverse momentum distributions, which are anomalous in the data. We use three techniques of increasing complexity to estimate the sensitivity to the details of modeling the kinematics. In the first method, we ignore entirely the kinematics of the primary lepton and the missing energy, and we model the jet kinematics with the fictitious production of a heavy state N of mass $220 \text{ GeV}/c^2$ which decays into $\tilde{b}\bar{\tilde{b}}$ according to phase space. This mechanism is chosen to reproduce the hard E_T spectrum of the superjet and the other jets in the final state, as well as their invariant mass distribution. The observed rates of tagged events are fitted with a SM simulation implemented with the additional production $p\bar{p} \rightarrow N \rightarrow \tilde{b}\bar{\tilde{b}}$ (described in Appendix A). Since this model is the simplest, we describe the fit in some detail in subsection A. Using the result of this fit, subsections B-D show that the addition of this hypothetical process improves the simulation of other peculiar features of the events with a superjet.

A. Fit of the tagging rates

We fit the rates of $W + n$ jet events ($n=1,4$) before and after tagging with the SM simulation implemented with the N production using a likelihood technique. In order to use all the information contained in the data, we fit nine ($k = 1, 9$) different classes of tagged events: events with one and two SECVTX tags; events with one and two JPB tags; events with one and two SLT tags; events with one supertag; events with one supertag and an additional SECVTX tag; and events with one SLT and one SECVTX tag in two different jets. In total we fit 31 data points.

The $t\bar{t}$ cross section and the number of events due to N production are unconstrained parameters of the fit, which has 29 degrees of freedom. The remaining eleven contributions

X_j to the tagging rates [SECVTX, JPB and SLT mistags, WW , WZ , ZZ , single top, Wc , Wcc , Wbb and unidentified- Z with heavy flavors] are also fit parameters. However, we constrain each contribution to its expected value, \bar{X}_i , and within its estimated uncertainty, $\sigma_{\bar{X}_i}$, using in the log-likelihood function the term

$$G_i = -\frac{(X_i - \bar{X}_i)^2}{2\sigma_{\bar{X}_i}^2}.$$

The detector acceptance, the luminosity and the values of the SECVTX, JPB and SLT tagging efficiencies are five additional fit parameters, which are also constrained to their measured value within their uncertainties.

In summary the fit minimizes the function

$$-\ln \mathcal{L} = -\sum_{n=1}^4 \sum_{k=1}^9 \ln P_{nk}(N_{nk}|\bar{\mu}_{nk}) - \sum_{i=1}^{16} G_i$$

where P_{nk} is the Poisson probability of observing N_{nk} events when $\bar{\mu}_{nk}$ events are expected.

The minimum value of $-\ln \mathcal{L}$ returned by the fit is -1854.7. If each data point were equal to the best fit result, we would have found $-\ln \mathcal{L}_0 = -1868.7$. The difference between $-\ln \mathcal{L}$ and $-\ln \mathcal{L}_0$ corresponds to a χ^2 increase of 28 units for 29 degrees of freedom. Rates of observed and fitted $W + \geq 1$ jet events before and after tagging are compared in Tables I to III.

The value of the $t\bar{t}$ cross section returned by the fit is 4.0 ± 1.5 pb, in agreement with theoretical expectations [10] and the DØ result [11]. This cross section corresponds to the presence of 41.9 ± 15.7 top events in the $W + \geq 1$ jet sample before tagging. In the same $W + \geq 1$ jet sample, the fit returns 52.8 ± 22.1 events due to the production of a massive $\tilde{b}\bar{b}$ pair. We quote numbers of events and not a cross section since the lepton and missing energy kinematics have been ignored.

TABLE I. Composition of the $W + \geq 1$ jet sample before tagging. This composition is determined by a fit to the tagging rates of the data (see text).

Source	$W + 1 \text{ jet}$	$W + 2 \text{ jet}$	$W + 3 \text{ jet}$	$W + \geq 4 \text{ jet}$
Data	9454	1370	198	54
Non- W	560.0 ± 15.1	71.2 ± 2.6	12.3 ± 2.0	5.1 ± 1.6
WW, WZ, ZZ	35.8 ± 7.6	36.2 ± 7.7	6.2 ± 1.3	0.9 ± 0.2
Unidentified- $Z + \text{jets}$	234.8 ± 14.5	38.5 ± 5.9	7.9 ± 2.4	0.7 ± 0.7
Single top	14.0 ± 2.2	7.8 ± 1.3	1.7 ± 0.3	0.3 ± 0.1
$t\bar{t}$	1.4 ± 0.5	7.9 ± 3.0	15.9 ± 6.0	16.7 ± 6.3
$W + \text{jets without h.f.}$	7955.8 ± 73.6	1004.5 ± 20.5	110.6 ± 6.6	19.1 ± 4.9
Wc	399.2 ± 89.1	82.1 ± 18.3	10.0 ± 2.2	1.8 ± 0.4
$Wc\bar{c}$	171.6 ± 36.9	60.1 ± 12.9	10.4 ± 2.2	2.2 ± 0.5
$Wb\bar{b}$	67.6 ± 7.8	28.8 ± 3.3	5.1 ± 0.6	1.4 ± 0.2
N	2.2 ± 0.9	28.2 ± 11.8	16.7 ± 7.0	5.6 ± 2.3

TABLE II. Summary of observed and fitted number of W events with one (ST) and two (DT) tags of the same kind (SECVTX, JPB, or SLT). “Other” is the sum of all processes other than $t\bar{t}$ and the fictitious N production (see text).

Source	$W + 1\text{jet}$	$W + 2\text{jet}$	$W + 3\text{jet}$	$W + \geq 4\text{jet}$
SECVTX tags				
Other (ST)	63.68 ± 3.89	25.60 ± 1.64	5.73 ± 0.39	1.45 ± 0.13
Other (DT)		1.56 ± 0.23	0.30 ± 0.04	0.07 ± 0.01
$t\bar{t}$ (ST)	0.42 ± 0.12	2.59 ± 0.74	5.25 ± 1.50	5.75 ± 1.65
$t\bar{t}$ (DT)		0.58 ± 0.17	2.22 ± 0.63	3.05 ± 0.87
N (ST)	0.21 ± 0.06	9.32 ± 2.75	6.20 ± 1.83	2.01 ± 0.59
N (DT)		3.08 ± 0.91	1.71 ± 0.51	0.70 ± 0.21
Fit (ST)	64.30 ± 3.90	37.50 ± 2.41	17.17 ± 1.50	9.21 ± 1.40
Fit (DT)	0.00 ± 0.00	5.22 ± 0.81	4.23 ± 0.54	3.81 ± 0.77
Data (ST)	66	35	10	11
Data (DT)	0	5	6	2
JPB tags				
Other (ST)	128.46 ± 9.36	45.77 ± 3.46	9.61 ± 0.78	2.06 ± 0.16
Other (DT)		1.54 ± 0.23	0.28 ± 0.04	0.06 ± 0.01
$t\bar{t}$ (ST)	0.41 ± 0.12	2.46 ± 0.73	5.12 ± 1.51	5.46 ± 1.61
$t\bar{t}$ (DT)		0.56 ± 0.17	2.02 ± 0.60	2.81 ± 0.83
N (ST)	0.24 ± 0.08	9.60 ± 2.97	5.70 ± 1.76	1.79 ± 0.55
N (DT)		3.20 ± 1.00	1.93 ± 0.60	0.75 ± 0.23
Fit (ST)	129.12 ± 9.44	57.83 ± 5.20	20.43 ± 2.66	9.31 ± 1.82
Fit (DT)		5.30 ± 0.94	4.23 ± 0.63	3.62 ± 0.76
Data (ST)	125	62	21	12
Data (DT)		6	5	3
SLT tags				
Other (ST)	140.55 ± 7.47	45.41 ± 2.38	10.13 ± 0.55	3.72 ± 0.22
Other (DT)		0.08 ± 0.01	0.01 ± 0.00	0.00 ± 0.00
$t\bar{t}$ (ST)	0.10 ± 0.03	1.02 ± 0.32	2.16 ± 0.68	2.55 ± 0.80
$t\bar{t}$ (DT)		0.03 ± 0.01	0.10 ± 0.03	0.13 ± 0.04
N (ST)	0.10 ± 0.03	8.07 ± 2.43	5.20 ± 1.56	1.75 ± 0.53
N (DT)		0.74 ± 0.22	0.41 ± 0.12	0.19 ± 0.06
Fit (ST)	140.75 ± 7.47	54.51 ± 2.99	17.49 ± 1.44	8.02 ± 0.77
Fit (DT)		0.86 ± 0.32	0.52 ± 0.17	0.32 ± 0.07
Data (ST)	146	56	17	8
Data (DT)		0	0	0

TABLE III. Summary of observed and fitted number of W events with one supertag (ST) and one supertag with an additional SECVTX tag (DT) (top table) and with one SLT and one SECVTX tag in two different jets (bottom table).

Source	$W + 1\text{jet}$	$W + 2\text{jet}$	$W + 3\text{jet}$	$W + \geq 4\text{jet}$
Other (ST)	3.77 ± 0.35	1.93 ± 0.18	0.54 ± 0.05	0.05 ± 0.00
Other (DT)		0.16 ± 0.02	0.03 ± 0.00	0.00 ± 0.00
$t\bar{t}$ (ST)	0.03 ± 0.00	0.29 ± 0.03	0.57 ± 0.05	0.70 ± 0.07
$t\bar{t}$ (DT)		0.07 ± 0.01	0.24 ± 0.02	0.37 ± 0.03
N (ST)	0.02 ± 0.00	1.54 ± 0.14	1.02 ± 0.10	0.28 ± 0.03
N (DT)		1.08 ± 0.10	0.63 ± 0.06	0.28 ± 0.03
Fit (ST)	3.82 ± 0.36	3.76 ± 0.35	2.13 ± 0.20	1.03 ± 0.10
Fit (DT)		1.31 ± 0.12	0.90 ± 0.08	0.65 ± 0.06
Data (ST)	1	6	2	2
Data (DT)		2	3	0
Source	$W + 1\text{jet}$	$W + 2\text{jet}$	$W + 3\text{jet}$	$W + \geq 4\text{jet}$
Other		1.10 ± 0.10	0.44 ± 0.04	0.20 ± 0.02
$t\bar{t}$		0.22 ± 0.02	0.60 ± 0.04	0.92 ± 0.06
N		1.17 ± 0.11	0.89 ± 0.08	0.32 ± 0.03
Fit		2.49 ± 0.23	1.93 ± 0.18	1.44 ± 0.14
Data		1	0	1

B. Choice of the N mass

The additional production $N \rightarrow \tilde{b}\bar{b}$ is a simple model capable of reproducing the observed yield of tagged events as a function of the jet multiplicity (see Tables II and III). Since the tagging rates are not very sensitive to the N mass, we have chosen its value after comparing the invariant mass distribution of jet pairs in the data and in the simulation. For this purpose, we have added to the original 13 events the four additional events with a superjet listed in Tables XVIII and XIX of Ref. [1]. Of these 17 events, 11 events contain only two jets. In the remaining 6 events with three jets, when possible, we combine the superjet with the other jet tagged by SECVTX (3 events). If no additional jets are tagged, we select the one with the highest transverse energy (3 events). In simulated events due to N production containing two untagged jets in addition to the superjet, the highest- E_T jet is produced by a parton from the N -decay in 77% of the cases.

Using the normalization provided by the fit in Section II A, the simulation predicts 10.2 events with a supertag: 6.0 ± 0.6 are due to N production, 1.3 ± 0.1 are due to $t\bar{t}$ production and 2.9 ± 0.3 are due to the remaining processes. Figure 1 compares the observed and predicted invariant mass distributions. A Kolmogorov-Smirnov (K-S) test of these distributions, described in detail in Section VII C of Ref. [1], yields a distance $\delta^0 = 0.37$ and a probability $P = 10.3\%$. The result of the K-S comparison of the di-jet invariant mass distributions in the data and in the simulation for several M_N values is also shown in Figure 1 (the probability P of the K-S test has been converted into a χ^2 per degree of freedom). In conclusion, the kinematics of the data is compatible with the additional production of a pair of $\tilde{b}\bar{b}$ partons with an average invariant mass of about 220 GeV/ c^2 .

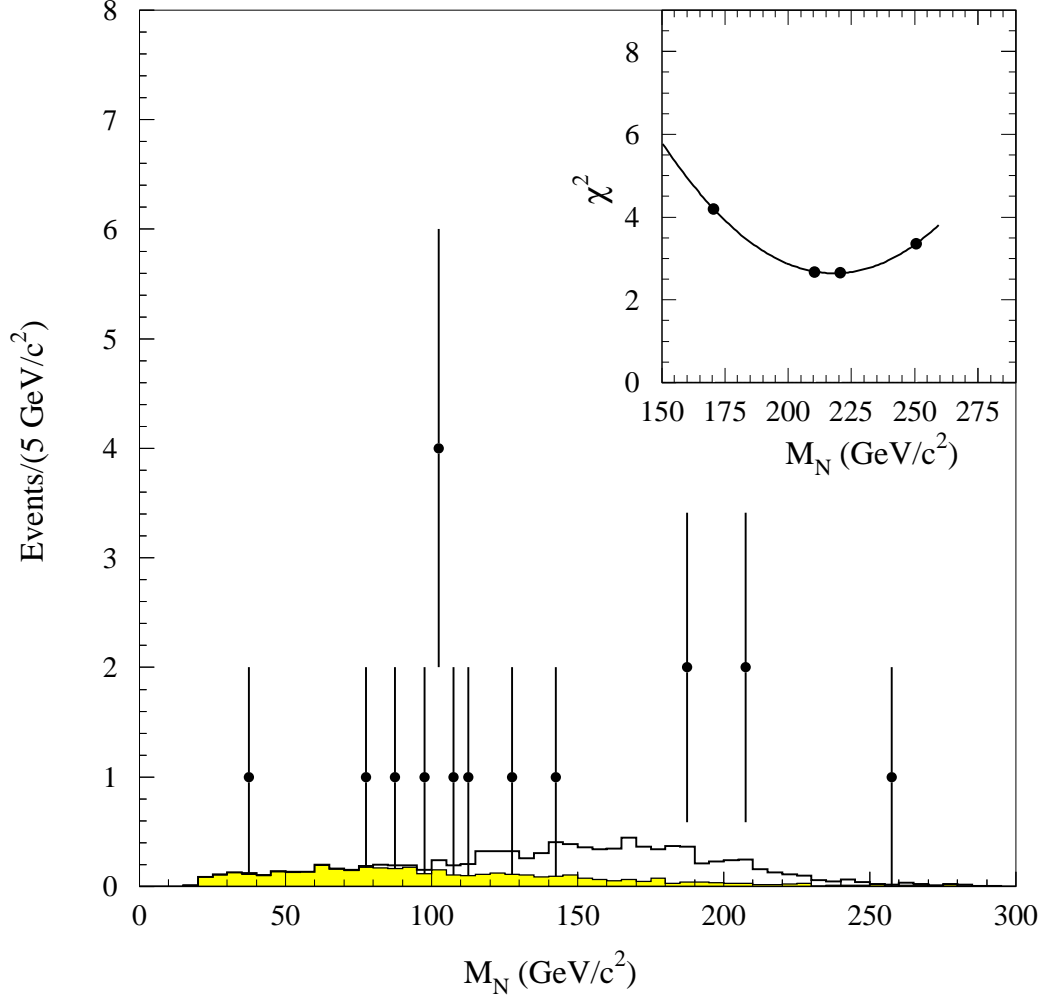


FIG. 1. Di-jet invariant mass distribution in the 17 events with a superjet (\bullet) and in the simulation implemented with the production of a state $N \rightarrow \tilde{b}\bar{b}$ with a $220 \text{ GeV}/c^2$ mass (histogram); the SM contribution is represented by the shaded histogram. The inset shows the yield of the reduced χ^2 of the comparison between the di-jet invariant mass distributions in the data and in the simulation as function of M_N .

C. Transverse momentum of the soft lepton tags

As discussed in Section IX B of Ref. [1], the distribution of the transverse momentum of the soft lepton tag, p_T^{SLT} , in the original 13 events with a superjet is quite anomalous, and

has a $P = 0.09\%$ probability of being consistent with the SM prediction. Figure 2(a) shows the p_T^{SLT} distribution in 15 events with a superjet (we add the two events recovered using primary plug electrons listed in Table XIX of Ref. [1] but not the two events triggered by the soft muons because of the trigger p_T -cut). The probability that the p_T^{SLT} distribution for these 15 events is consistent with the SM simulation remains small ($P = 0.1\%$). The K-S comparison of the p_T^{SLT} distribution to a SM simulation implemented with the N production (Figure 2(a)) yields a distance $\delta^0 = 0.34$ and a probability $P = 11.8\%$. The improved agreement obtained by adding the N -production can be understood from the comparison of the p_T^{SLT} distributions in SM processes and in events due to the N production in which most of the soft leptons are produced by \tilde{b} decays (Figure 2(b)).

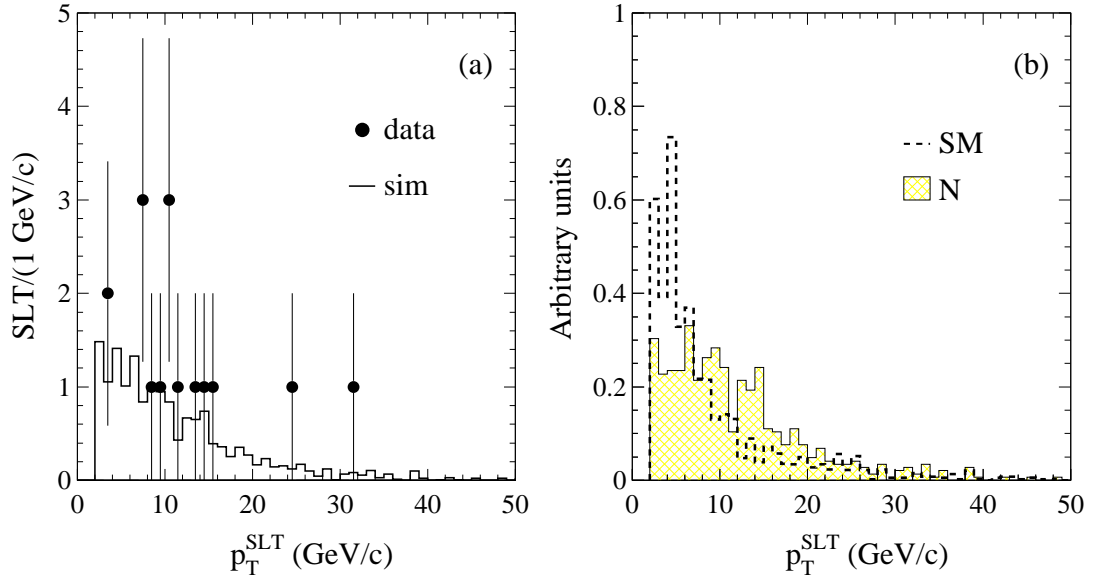


FIG. 2. Distributions (a) of the transverse momentum of soft lepton tags in the 15 events with a superjet and in simulated events which include the $N \rightarrow \tilde{b}\bar{b}$ production. The SM and the N contributions, normalized to the same number of events, are also shown (b) separately.

D. Charge correlation between the primary lepton and the soft lepton in the superjets

In 13 out of 17 events with a superjet, listed in Tables XVI to XIX of Ref. [1], the charges of the primary lepton and the soft lepton tag are opposite. SM processes which contribute to events with a superjet do not produce a visible charge correlation; the binomial probability of an equal or larger statistical fluctuation is 2.4%.

In the $N \rightarrow \tilde{b}\bar{b}$ simulation most superjets are produced by semileptonic \tilde{b} -decays. In 67% of the cases, the soft lepton charge has the same sign of the \tilde{b} charge. According to the fit in Section II A, 4.2 of the 17 events are attributed to SM processes which do not produce a visible charge correlation. If the remaining 12.8 events with a superjet represent the final state $(\tilde{b}\bar{b}) + l^+ + \cancel{E}_T$ (and its charge-conjugate), in which the charges of the primary lepton and the \tilde{b} quark are opposite, then in 17 events we expect to find 10.7 events in which the primary and soft lepton have opposite charge. The probability that the data are generated according to this hypothesis increases from 2.4% to 18.6%.

III. ESTIMATE OF THE ACCEPTANCE FOR EVENTS WITH A SUPERJET

The fit in the Section II A returns 52.8 ± 22.1 events not attributed to SM processes. In order to turn this number into a cross section we try two phenomenological approaches to estimate the detector acceptance. We first use a W + Higgs boson simulation where we identify the Higgs with the state N which decays to $\tilde{b}\bar{b}$. As detailed in Appendix B, we arbitrarily weight the angular distribution of the primary lepton to obtain an approximate agreement with the data. Although, as shown in Appendix B, the remaining kinematics is poorly modeled by the hypothesis of a final state containing two massive particles (W and N), this simulation provides a jet multiplicity distribution consistent with the simpler N production. A fit of the rates of tagged W + jet events with the SM simulation implemented with this WN production also returns a number of tagged WN events consistent with the

fit shown in Tables II and III. The detector acceptance for such a WN process is about 9% without including the W leptonic branching ratio.

In a second attempt to evaluate the detector acceptance, we model the production of events with a superjet with a more general $2 \rightarrow 4$ hard scattering process. As detailed in Appendix C, the matrix element of this process is tuned using an effective Lagrangian approach to account for the salient kinematic features of the data. In this picture the primary lepton and the missing energy do not come from W decays. In this simulation, the yield of events before and after tagging as a function of the jet multiplicity is similar to that of the $p\bar{p} \rightarrow N$ simulation (Tables I to III). Under the assumption that the lepton in the final state can be an electron, a muon or a τ with equal probability, the detector acceptance for this simulated process is 10.8%, consistent with the WN simulation.

If we average the two techniques for estimating the detector acceptance, then the 52.8 ± 22.1 events with a superjet required by the fit in Table I correspond to a cross section of about 5 ± 2 pb.

IV. CONCLUSIONS

We present additional studies of the kinematics of the anomalous events with a superjet observed by CDF. We model several properties of the superjets with the hypothesis of the production and decay of a light scalar quark. Using phenomenological approaches, based on this ansatz, to evaluate the detector acceptance and the tagging efficiencies for events with a superjet, we estimate that their production cross section is approximately 5 ± 2 pb, independent of the details of the kinematic distributions. At the same time, we derive a new estimate of the $t\bar{t}$ cross section value, 4.0 ± 1.5 pb, using $W + \geq 1$ jet events with SECVTX, JPB and SLT tags. This result agrees with the $D\bar{O}$ measurement [11], $\sigma_{t\bar{t}} = 4.1 \pm 2.0$ pb, derived in the same topological channel by using kinematical cuts designed to select $t\bar{t}$ events.

ACKNOWLEDGMENTS

We thank the Fermilab staff and the CDF collaboration for their contributions. We are grateful to Stefano Moretti for implementing new processes into the HERWIG generator and to H. Georgi, S. Glashow, H. Logan, M. Mangano, and J. Terning for many interesting and helpful conversations. This work was supported by the U.S. Department of Energy, the National Science Foundation and the Istituto Nazionale di Fisica Nucleare.

APPENDIX A: SIMULATION OF THE PROCESS $p\bar{p} \rightarrow N$

We simulate the process $p\bar{p} \rightarrow N$ with the HERWIG Monte Carlo program [12]. We produce the state N using option 1605, which calculates the production of a Higgs boson in $p\bar{p}$ interactions. The Higgs boson is forced to decay to $b\bar{b}$. The decay of the \bar{b} -hadron formed by HERWIG is performed using the QQ Monte Carlo program [13]. The b -quark is transformed into a scalar quark in the following way. Having modified the HERWIG generator, we set the b -quark mass to 3.6 GeV/c². The b -quark is hadronized by HERWIG as a fermion. At the end of the hadronization process, when a b -hadron has been formed, we change its identity to a fictitious \tilde{b} -hadron, but we keep the hadron mass evaluated by HERWIG at this stage. The decay of the \tilde{b} -hadron is modeled with HERWIG using the spectator model (routine HWDHVV). In this model, HERWIG weights in the routine HWDHQK the phase space of the three-body semileptonic decay of a b -quark with the V-A matrix element calculated with the routine HWDWWT. In the case of a scalar quark we modified HERWIG to weight the phase-space with the matrix element:

$$\frac{d\Gamma}{dz_c dz_l} = K[(1 - z_c)(1 - z_l) - R_{\tilde{\nu}} + R_c(z_c - z_l + R_{\tilde{\nu}} - R_c)] \quad (\text{A1})$$

where K is a normalization factor, $R_c = m_c^2/m_b^2$ and $R_{\tilde{\nu}} = m_{\tilde{\nu}}^2/m_b^2$.

Here z_c and z_l are defined as

$$z_c = \frac{2p_{\tilde{b}} \cdot p_c}{m_b^2} \quad \text{and} \quad z_l = \frac{2p_{\tilde{b}} \cdot p_l}{m_b^2}$$

The phase space limits are:

$$2\sqrt{R_c} < z_c < 1 + R_c - R_{\tilde{\nu}}$$

$$\frac{1 + R_c - R_{\tilde{\nu}} - z_c}{1 - [z_c - \sqrt{z_c^2 - 4R_c}]/2} < z_l < \frac{1 + R_c - R_{\tilde{\nu}} - z_c}{1 - [z_c + \sqrt{z_c^2 - 4R_c}]/2}$$

This matrix element for the decay $\tilde{b} \rightarrow cl\tilde{\nu}$ is derived from the tree level calculation outlined in Ref. [14]

$$\mathcal{M} = \sum_{j=1}^2 \frac{-g^2 V_{j1} F_L |V_{c\tilde{b}}|}{(p_{\tilde{b}} - p_c)^2 - m_{\chi_j}^2} \left[\left[U_{j1} \cos\theta - \frac{m_b U_{j2} \sin\theta}{\sqrt{2} m_W \cos\beta} \right] m_{\chi_j} \bar{u}(p_c) P_R v(p_l) + \frac{m_c V_{j2}^* \cos\theta}{\sqrt{2} m_W \sin\beta} \bar{u}(p_c) \not{p}_{\tilde{\nu}} P_R v(p_l) \right] \quad (\text{A2})$$

where χ_j 's are the chargino mass eigenstates, and U and V^* are the mixing matrices for the right and left-handed charginos, respectively. The first subscript of U , V corresponds to mass eigenstates and the second to weak eigenstates (1 for the gaugino and 2 for the higgsino). Here $\tan\beta$ is the ratio of the vacuum expectation values of the two Higgs fields, θ is the mixing angle between left-handed and right-handed scalar quarks, F_L is the fraction of left-handed component of the scalar neutrino, and $|V_{c\tilde{b}}|$ is the CKM matrix element. Equation (A1) follows from (A2) when the decay is mediated by the higgsino coupling to the right-handed matter. If the decay is mediated by the gaugino coupling to the left-handed matter the matrix element is

$$\frac{d\Gamma}{dz_c dz_l} = K(z_c + z_l - 1 + R_{\tilde{\nu}} - R_c). \quad (\text{A3})$$

In the latter case the two fermions in the final state are both left-handed and tend to be produced back-to-back since the initial state is spinless. Using equation (A1) the two fermions in the final state have opposite handedness and tend to be produced more collinear than when using equation (A3). It follows that the matrix element (A1) produces leptons with a momentum distribution appreciably softer than when using the matrix element (A3) or a phase space decay, as done in Ref. [8]. The c -quark emerging from the \tilde{b} -quark decay is then recombined in HERWIG with the spectator quark by the routine HWCFOR. The decay of the resulting c -hadron is performed with the QQ Monte Carlo program. In the spectator

model, excited D -meson states are produced only by the hadronic current carried by the virtual W (so called *upper vertex*). Since we impose that the gauge fermion involved in the scalar quark decay has only leptonic decay modes, the simulation produces a very simple list of c -hadrons with respect to the QQ generator (see Figure 3).

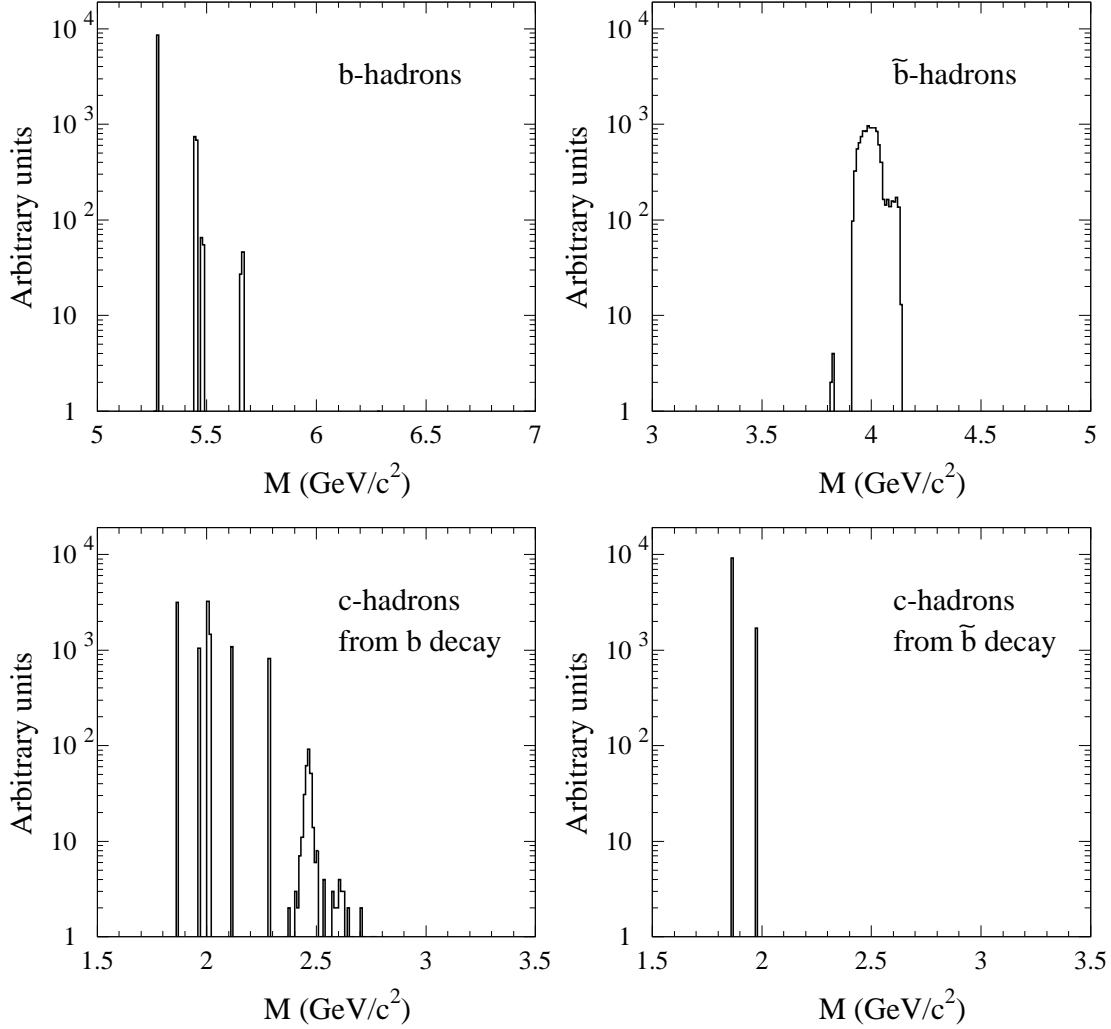


FIG. 3. Mass spectrum of the b and \tilde{b} -hadrons produced by the HERWIG simulation using $m_b=4.75$ GeV/c² (a) and $m_{\tilde{b}}=3.65$ GeV/c² (b). (c): mass spectrum of the c -hadrons from b -hadron decays modeled with QQ. (d): mass spectrum of the c -hadrons from \tilde{b} -hadron decays modeled with the HERWIG spectator model.

APPENDIX B: SIMULATION OF THE PROCESS $p\bar{p} \rightarrow WN$

We generate the process $q_i\bar{q}_j \rightarrow WH$ with $m_H = 220 \text{ GeV}/c^2$ using option 2605 of HERWIG and the MRS(G) set of structure functions [15]. We identify the Higgs boson with the state N and we force it to decay to $\tilde{b}\bar{b}$. As shown in Figure 4, the distributions of the pseudo-rapidity and transverse momentum of primary leptons in this simulation and in the data are quite different. We attempt to model the data by considering the process $q_i\bar{q}_j \rightarrow WN$ as a $2 \rightarrow 3$ hard scattering ($q_i\bar{q}_j \rightarrow l^+\cancel{E}_T N$, with subsequent decay $N \rightarrow \tilde{b}\bar{b}$). For the sake of simplicity, we ignore the polarization of the outgoing W calculated by HERWIG and decay the W boson into $l\nu$ according to two-body phase space. Then, in order to model the observed pseudo-rapidity distribution of the primary leptons, we weight their distribution in the $q_i\bar{q}_j$ rest-frame with the function $z^4 = \cos^4 \theta_l$, where θ_l is the polar angle of the primary lepton with respect to the q_i -direction. As shown in Figure 5, this attempt is quite successful.

Using this simulation, we compare additional kinematical quantities to the data. Figure 6 shows the correlation between the pseudo-rapidity of the primary lepton and the rapidity of the di-jet system N . In the simulation, in which the W boson recoils against the state N , primary leptons tend to have rapidities opposite to the N direction. In the data, the N rapidity is quite central, independent of the primary lepton pseudo-rapidity. In the data, primary leptons are produced at large rapidities while the state N is produced quite centrally; therefore, most of the N transverse momentum is balanced by the missing transverse energy (Figure 7).

Pseudo-rapidity distributions of the b -jets in the data and in the WN simulation are shown in Figure 8. Differently from the small sample of data, simulated b -jets produced by the decay of a massive state N tend to fill quite uniformly the η -region covered by the detector.

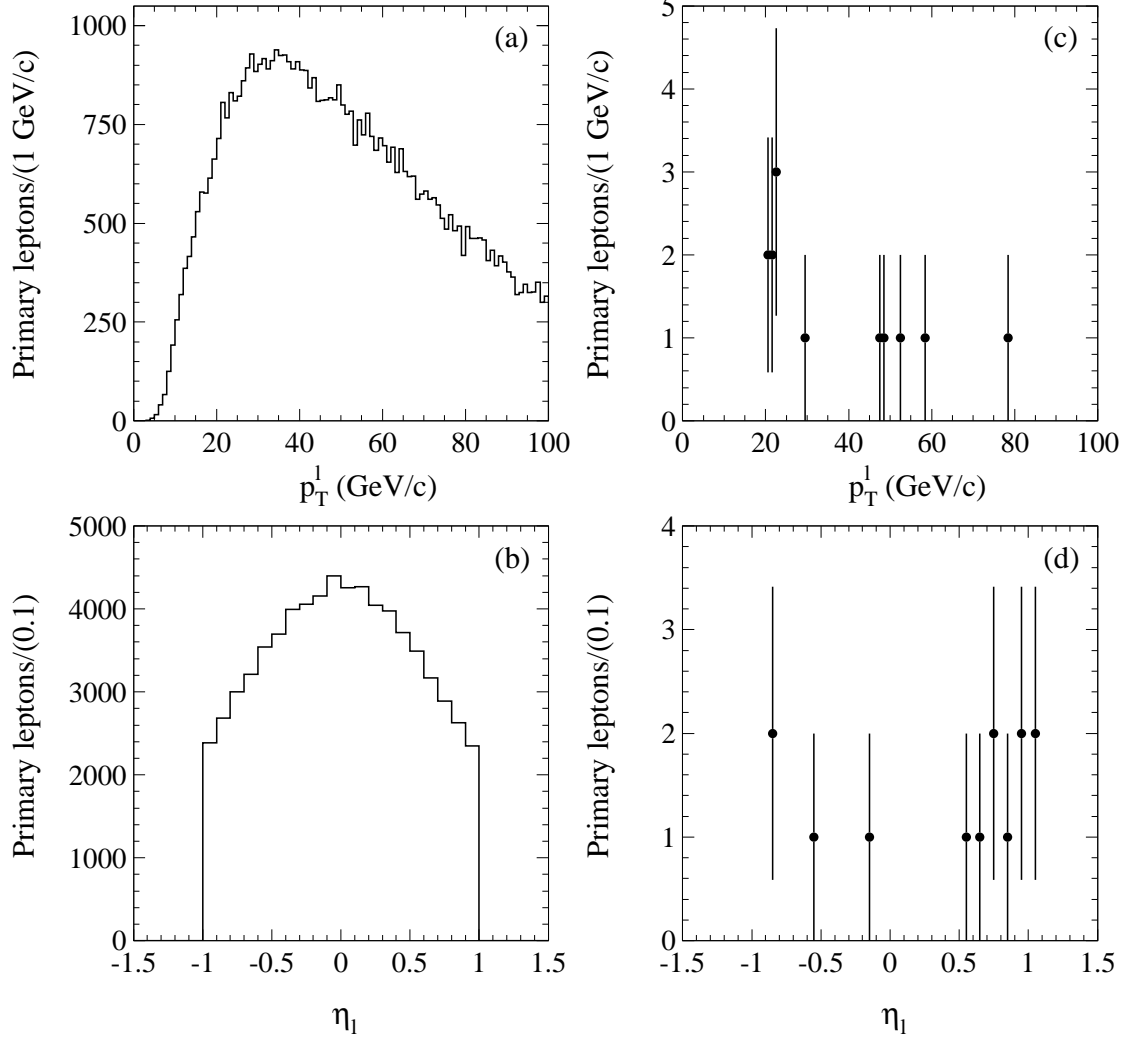


FIG. 4. Transverse momentum (a) and pseudo-rapidity (b) distributions of the primary leptons resulting from the decay of W bosons produced in association with a Higgs of mass $220 \text{ GeV}/c^2$; (c) and (d) are the analogous distributions for the data.

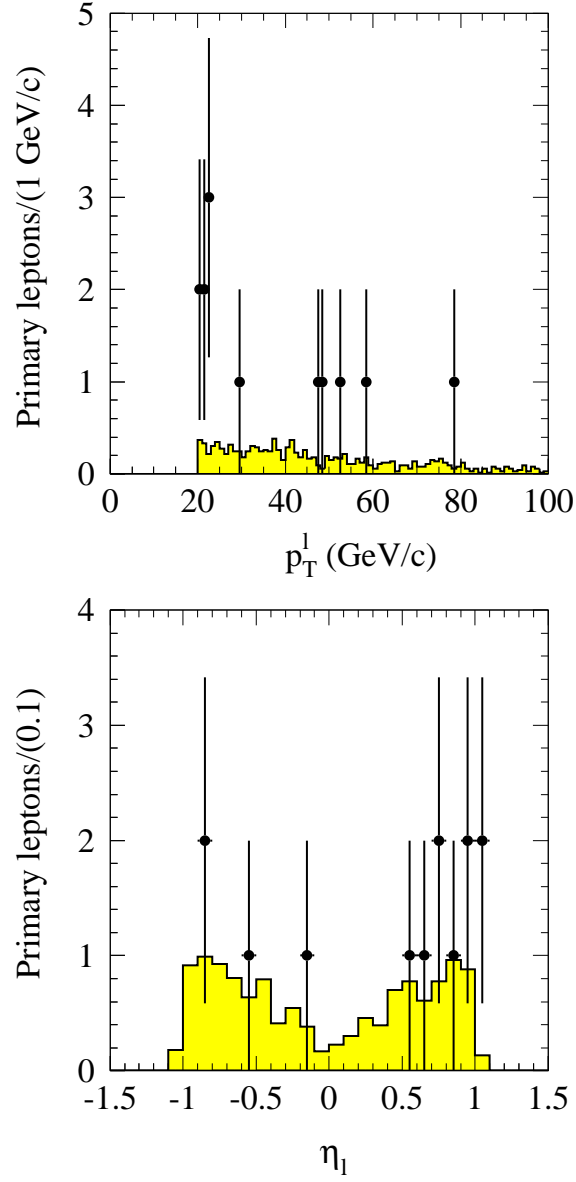


FIG. 5. Transverse momentum and pseudo-rapidity distributions of the primary lepton. The data (\bullet) are compared to a $q_i \bar{q}_j \rightarrow l \cancel{E}_T N$ simulation in which the angular distribution of the primary lepton is weighted with the function $\cos^4 \theta_l$ (see text).

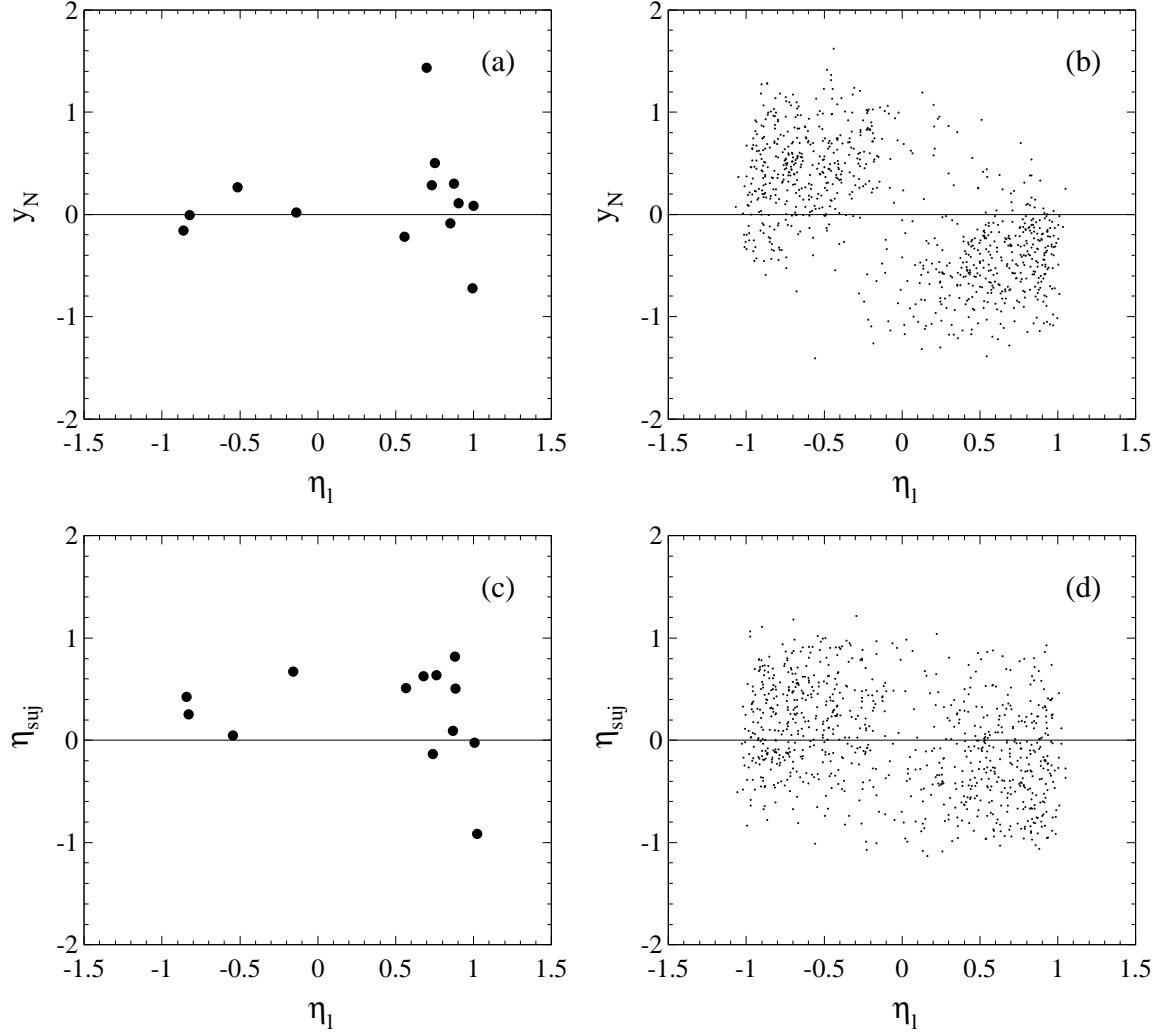


FIG. 6. Distribution of the rapidity y_N vs the pseudo-rapidity η_l of the primary lepton in the data (a) and in the modified WN simulation (b). The distribution of the pseudo-rapidity η_{suj} of the superjets versus η_l is shown in (c) for the data and in (d) for the simulation.

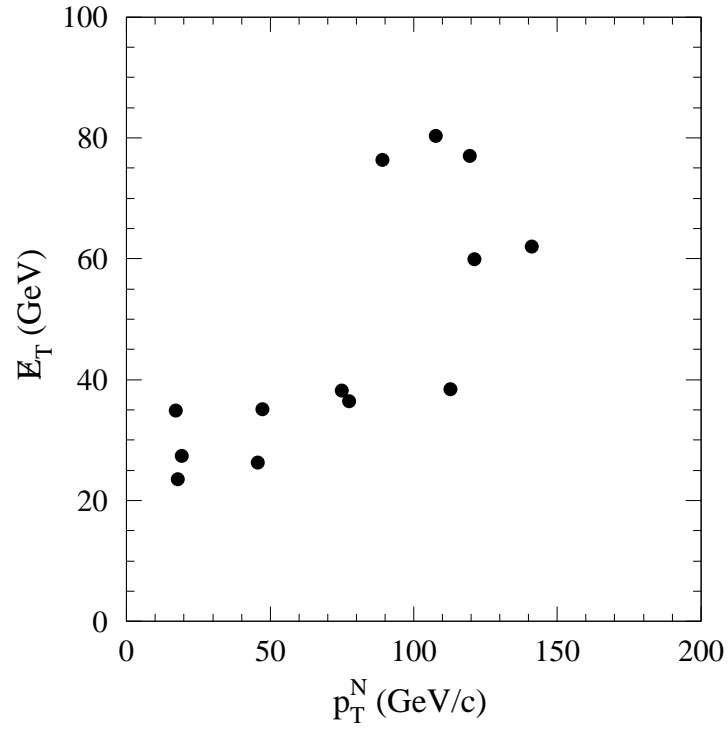


FIG. 7. Distribution of E_T vs p_T^N in the 13 events with a superjet.

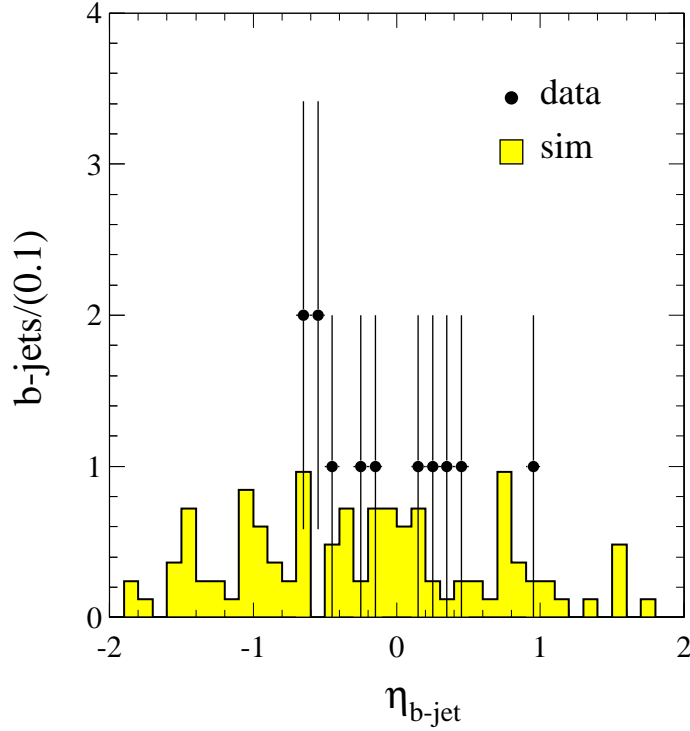


FIG. 8. Pseudo-rapidity distributions of b -jets in the data (\bullet) and in the WN simulation (shaded histogram).

APPENDIX C: EFFECTIVE LAGRANGIAN APPROACH

The matrix element used in Sec. III has been derived using an effective Lagrangian approach to incorporate the salient features of the data. The production of events with a superjet is modeled with the $2 \rightarrow 4$ hard scattering process

$$u(p_1) + \bar{d}(p_2) \rightarrow e^+(p_l) + \nu_s(k) + \bar{b}(p_b) + b_s(p_s) \quad (\text{C1})$$

where b_s and ν_s are a scalar quark and a scalar neutrino. A scalar neutrino is used in the final state to model the measured missing energy for no compelling reason other than the fact that we have already identified superjets with a scalar quark.

One mechanism capable of producing a z^4 angular distribution for the primary leptons in the final state is a high derivative coupling to the lepton and quark fields. As a first step, using the scalar fields ϕ of the ν_s and $\tilde{\phi}$ of the b_s , the following dimension-1 and spin-2 fields are constructed:

$$\phi_{\mu\nu}(x) = (1/\Lambda)^2 \partial_\mu \partial_\nu \phi(x) \text{ and } \tilde{\phi}_{\mu\nu} = (1/\Lambda)^2 \partial_\mu \partial_\nu \tilde{\phi}(x)$$

where Λ sets the mass scale of the interaction. In analogy, from the lepton and quark spinors one constructs the following dimension-3/2 and spin-5/2 fields:

$$\psi_l^{\mu\nu}(x) = (1/\Lambda)^2 \partial^\mu \partial^\nu \psi_l(x); \psi_b^{\mu\nu}(x) = (1/\Lambda)^2 \partial^\mu \partial^\nu \psi_b(x)$$

and

$$\begin{aligned} \chi_q^{\mu\nu}(x) &= (1/\Lambda)^2 \partial^\mu \partial^\nu \left[\frac{1+s_q}{2} \psi_u(x) + \frac{1-s_q}{2} \psi_d(x) \right] \\ \xi_q^{\mu\nu}(x) &= (1/\Lambda)^2 \partial^\mu \partial^\nu \left[\frac{1-s_q}{2} \psi_u(x) + \frac{1+s_q}{2} \psi_d(x) \right] \end{aligned}$$

where s_q is the sign of the initial state ($u + \bar{d}$) charge. The peculiar forms $\chi_q^{\mu\nu}$ and $\xi_q^{\mu\nu}$, used to account for the fields of the initial state partons, are an attempt to also model the asymmetries observed in the rapidity distributions of the data.

These fields are used to write the following high-derivative, but point-like, effective Lagrangian:

$$\mathcal{L}(x) = \left(\frac{f}{\Lambda_{10}}\right) \partial_\lambda \{ \phi_{\alpha\beta}^\dagger(x) \tilde{\phi}'_{\delta\phi}(x) \psi''^{\tau\sigma}_b(x) \} \gamma^\rho \partial^\lambda \{ \overset{\leftrightarrow}{\partial}^\omega \psi_l^{\mu\nu}(x) \overset{\leftrightarrow}{\partial}^\omega [(\partial_\tau \bar{\xi}_q^{\delta\phi}(x)) \gamma_\rho \overset{\leftrightarrow}{\partial}^\mu \overset{\leftrightarrow}{\partial}^\nu (\partial_\sigma \chi_q^{\alpha\beta}(x))] \}$$

where $A \overset{\leftrightarrow}{\partial}_\nu B = A(\partial_\nu B) - (\partial_\nu A)B$, and ψ'' is the transpose of ψ' , the “charge-conjugate” of ψ . To avoid conflict with unitarity in the high energy limit, we introduce a form factor to compensate for the twenty derivatives used above ¹. However, the effective Lagrangian

¹Since we use derivative couplings to fundamental fields, it is natural to assume that the hypothetical object involved in the s -channel exchange is composite.

acquires a reasonable s -behaviour only after the inclusion of an additional s -channel propagator. The squared amplitude for the process (C1) (and its charge conjugate), averaged over initial quark colors, then reads

$$|\mathcal{M}|^2 = \left(\frac{f}{\Lambda^2}\right)^2 \frac{\hat{s}^{13}}{(\hat{s} + \Lambda_1^2)^{20}} \frac{(E_b E_l)^5 (k E_s)^4}{(\hat{s} - M^2)^2 + M^2 \Gamma^2} [1 - \cos \vartheta_l \cos \vartheta_b] \times \quad (C2)$$

$$\left(1 - \frac{2E_l}{\sqrt{\hat{s}}}\right)^2 \left(1 - \frac{4E_l}{\sqrt{\hat{s}}}\right)^2 \left[\cos \vartheta_l \sin \vartheta_b \left(\frac{1 - \cos \vartheta_k}{2}\right) \left(\frac{1 + \cos \vartheta_s}{2}\right) \right]^4$$

In the kinematics of Eq. (C2), all six particles in the initial and final states are taken to be massless. The energies and polar angles $[(E_l, \vartheta_l)$ for the lepton, (E_b, ϑ_b) for the b-quark, (k, ϑ_k) for the scalar neutrino, and (E_s, ϑ_s) for the scalar b-quark] are defined in the $u\bar{d}$ center of mass system, and $u(p_1)$ is taken to be the in the z -direction. Such an effective Lagrangian has been constructed by iterations in which we compared data and simulation. We have started using a dimension-6 Lagrangian and we kept increasing the Lagrangian dimension till we obtained an acceptable description of the data.

The process (C1) has been kindly implemented into the HERWIG generator [16]. In the calculation of the matrix element (C2), we use $f = 1$ and $\Lambda_1 = 0$ GeV. In order to approximately reproduce the distribution of the invariant mass of the final state in the data, we use $M \simeq 350$ GeV/c² and $\Gamma \simeq 5$ GeV/c²². The cross section value of 5 pb derived in Sec. III corresponds to an interaction scale Λ of approximately 10 MeV.

Figures 9 to 11 compare pseudo-rapidity, transverse momentum and invariant mass distributions in the data and the simulation normalized to the same number of events. Data and simulation are in qualitatively good agreement.

²Widths Γ as large as 50 GeV/c² and masses M in the range of 300 – 400 GeV/c² also provide quite similar results.

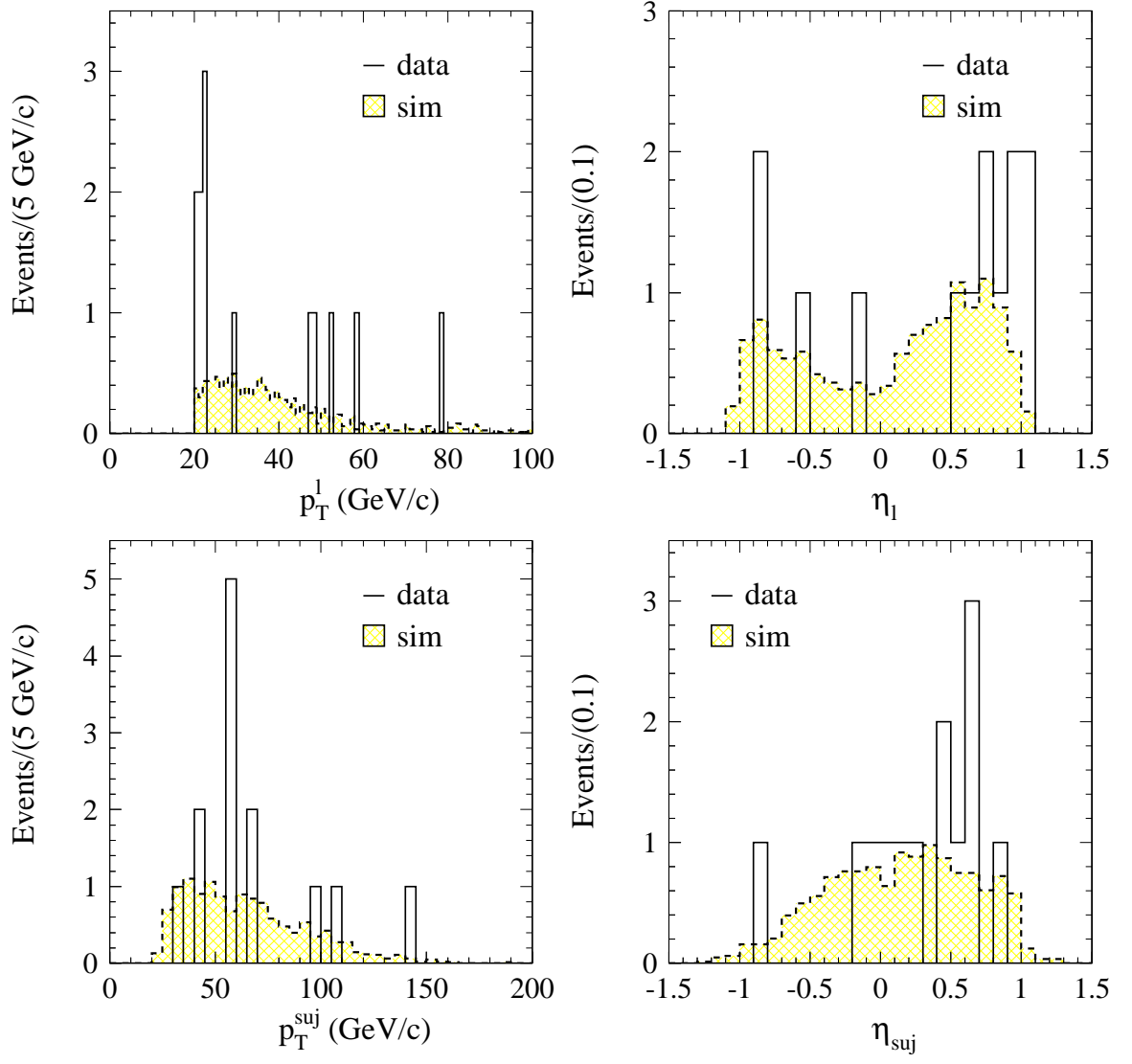


FIG. 9. Transverse momentum and pseudo-rapidity distributions of primary leptons and super-jets.

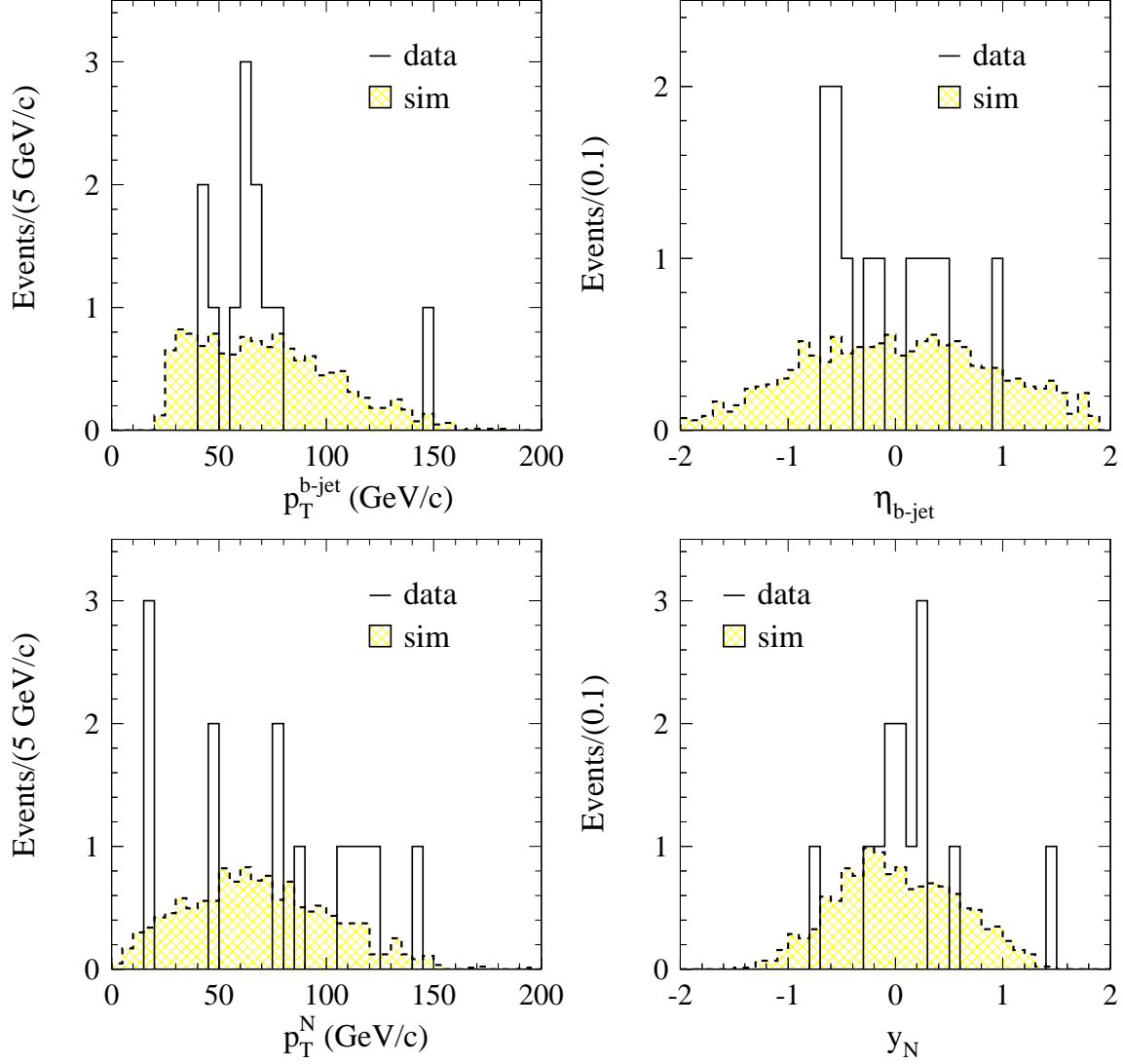


FIG. 10. Transverse momentum and rapidity distributions of b -jets and of the system N consisting of the b -jet and the superjet.

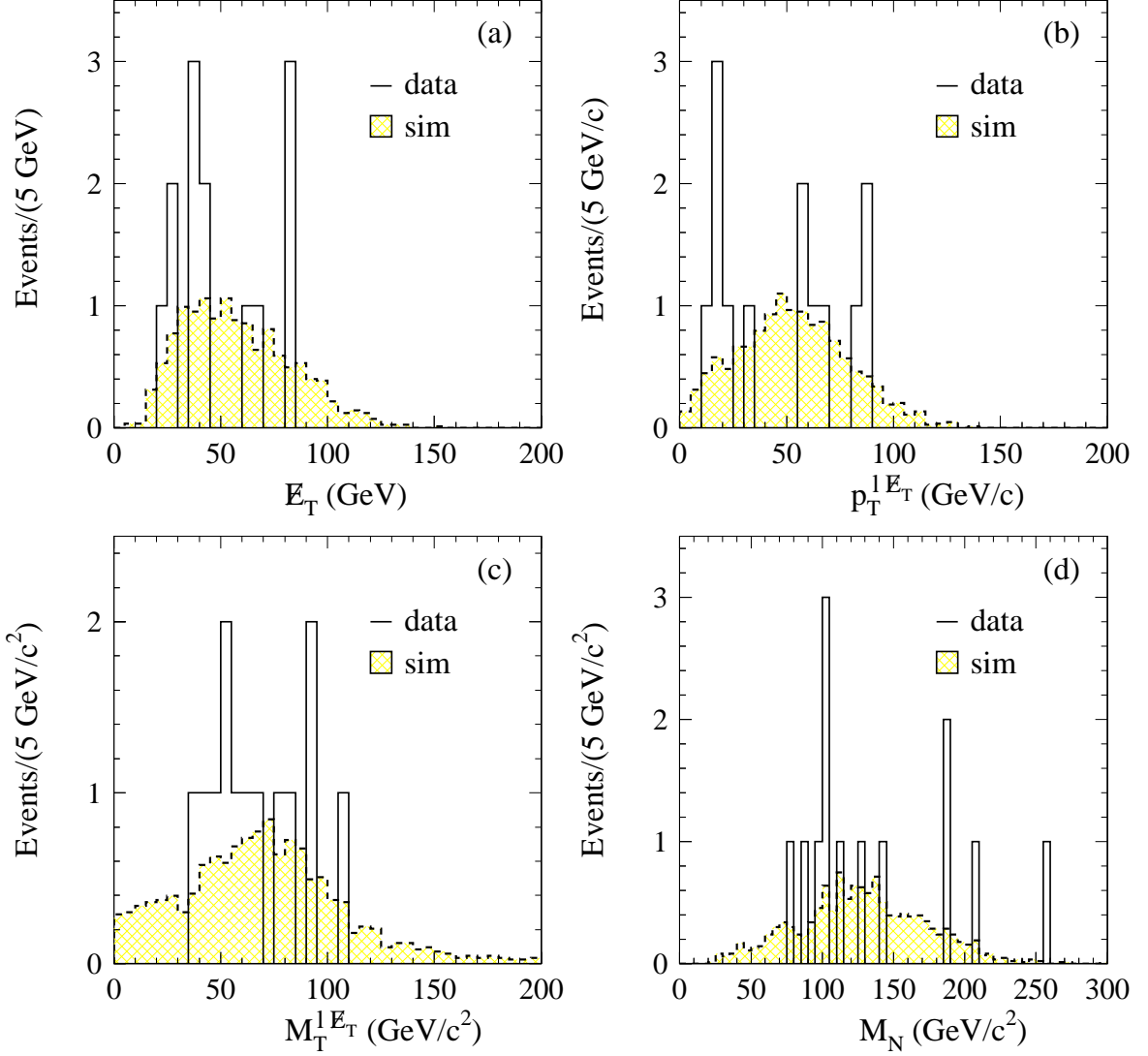


FIG. 11. Distributions of: E_T (a); the transverse momentum of the system lE_T composed by the primary lepton and the transverse missing energy (b); the transverse mass of the system lE_T (c); and the invariant mass of the system N consisting of the b -jet and the superjet (d).

-
- [1] D. Acosta *et al.*, hep-ex/0109012.
 - [2] G. Apollinari *et al.*, hep-ex/0109019.
 - [3] D. Buskulic *et al.*, Phys. Lett. **B313**, 535 (1993).
 - [4] T. Affolder *et al.*, Phys. Rev. **D64**, 032002 (2001).
 - [5] H. E. Haber and G. L. Kane, Phys. Rep. **117C**, 76 (1985).
 - [6] C. Nappi, Phys. Rev. **D25**, 84 (1982).
 - [7] M. Carena *et al.*, Phys. Rev. Lett. **86**, 4463 (2001).
 - [8] V. Savinov *et al.*, Phys. Rev. **D63**, 051101 (2001).
 - [9] A mass $m_{\tilde{\nu}}$ as large as 10 GeV/c² can be approximately excluded. In such a case, the energy of the scalar quark necessary to produce the observed transverse energy of the superjets would be about 200 GeV and, in contrast with the data, the observed missing transverse energy would always be pointing in the direction of the superjet.
 - [10] F. Bonciani *et al.*, Nucl. Phys. **B529**, 450 (1998); E. Berger and H. Contopanagos, Phys. Rev. **D54**, 3035 (1996); S. Catani *et al.*, Phys. Lett. **B378**, 329 (1996); E. Laenen *et al.*, Phys. Lett. **B321**, 254 (1994); P. Nason *et al.*, Nucl. Phys. **B303**, 607 (1998).
 - [11] S. Abachi *et al.*, Phys. Rev. Lett. **79**, 12003 (1997).
 - [12] G. Marchesini and B. R. Webber, Nucl. Phys. **B310**, 461 (1988); G. Marchesini *et al.*, Comput. Phys. Comm. **67**, 465 (1992).
 - [13] P. Avery, K. Read, G. Trahern, Cornell Internal Note CSN-212, March 25, 1985 (unpublished).
We use Version 9.1 of the CLEO simulation and our own lifetime database.
 - [14] K. Hikasa and M. Kobayashi, Phys. Rev. **D36**, 724 (1987); J. F. Gunion and H. E. Haber,

Nucl. Phys. **B272**, 1 (1986).

[15] A. D. Martin, R. G. Roberts and W. J. Stirling, Phys. Lett. **B354**, 155 (1995).

[16] The process (C1) has been implemented into the HERWIG simulation by S. Moretti (routine HWGRVT).